

Scintillation-only Based Pulse Shape Discrimination for Nuclear and Electron Recoils in Liquid Xenon

K.Ueshima^{a,*}, K.Abe^a, K.Hiraide^a, S.Hirano^a, Y.Kishimoto^{a,b},
K.Kobayashi^a, Y.Koshio^a, J.Liu^b, K.Martens^b, S.Moriyama^{a,b},
M.Nakahata^{a,b}, H.Nishiie^a, H.Ogawa^a, H.Sekiya^a,
A.Shinozaki^a, Y.Suzuki^{a,b}, A.Takeda^a, M.Yamashita^{a,b},
K.Fujii^c, I.Murayama^c, S.Nakamura^c, K.Otsuka^d,
Y.Takeuchi^{d,b}, Y.Fukuda^e, K.Nishijima^f, D.Motoki^f, Y.Itow^g,
K.Masuda^g, Y.Nishitani^g, H.Uchida^g, S.Tasaka^h, H.Ohsumiⁱ,
Y.D.Kim^j, Y.H.Kim^k, K.B.Lee^k, M.K.Lee^k, and J.S.Lee^k
the XMASS Collaboration

^a*Kamioka Observatory, Institute for Cosmic Ray Research, The University of
Tokyo, Kamioka, Gifu 506-1205, Japan*

^b*Institute for the Physics and Mathematics of the Universe, The University of
Tokyo, Kashiwa, Chiba 277-8582, Japan*

^c*Department of Physics, Faculty of Engineering, Yokohama National University,
Yokohama 240-8501, Japan*

^d*Department of Physics, Kobe University, Kobe, Hyogo 657-8501, Japan*

^e*Department of Physics, Miyagi University of Education, Sendai, Miyagi
980-0845, Japan*

^f*Department of Physics, Tokai University, Hiratsuka, Kanagawa 259-1292, Japan*

^g*Solar Terrestrial Environment Laboratory, Nagoya University, Nagoya, Aichi
464-8602, Japan*

^h*Department of Physics, Gifu University, Gifu, Gifu 501-1193, Japan*

ⁱ*Faculty of Culture and Education, Saga University, Honjo, Saga 840-8502, Japan*

^j*Department of Physics, Sejong University, Seoul 143-747, Korea*

^k*Korea Research Institute of Standards and Science, Daejeon 305-340, Korea*

Abstract

In a dedicated test setup at the Kamioka Observatory we studied pulse shape discrimination (PSD) in liquid xenon (LXe) for dark matter searches. PSD in LXe was based on the observation that scintillation light from electron events was emitted

over a longer period of time than that of nuclear recoil events, and our method used a simple ratio of early to total scintillation light emission in a single scintillation event. Requiring an efficiency of 50% for nuclear recoil retention we reduced the electron background to $7.7 \pm 1.1(\text{stat}) \pm_{0.6}^{1.2}(\text{sys}) \times 10^{-2}$ at energies between 4.8 and 7.2 keV_{ee} and to $7.7 \pm 2.8(\text{stat}) \pm_{2.8}^{2.5}(\text{sys}) \times 10^{-3}$ at energies between 9.6 and 12 keV_{ee} for a scintillation light yield of 20.9 p.e./keV. Further study was done by masking some of that light to reduce this yield to 4.6 p.e./keV, the same method results in an electron event reduction of $2.4 \pm 0.2(\text{stat}) \pm_{0.2}^{0.3}(\text{sys}) \times 10^{-1}$ for the lower of the energy regions above. We also observe that in contrast to nuclear recoils the fluctuations in our early to total ratio for electron events are larger than expected from statistical fluctuations.

Key words: Scintillation, Liquid xenon, Pulse shape discrimination
PACS: 29.40.Mc, 23.40.-s

1 Introduction

The results of various astronomical observations [1] - [5] show strong evidence for a large amount of dark matter in the universe. Weakly Interactive Massive Particles (WIMPs) are a dark matter candidate motivated in extensions of the theory of high energy particle physics [6]. Various dedicated WIMP dark matter search experiments are underway around the world [7] - [9]. The XMASS experiment, using liquid xenon (LXe) as a target for WIMP dark matter, was proposed in 2000 [10]. The construction of the 800 kg detector was finished in 2010.

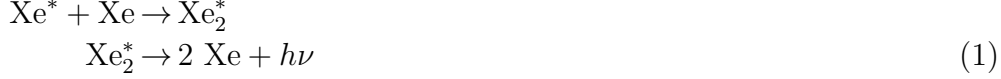
The interaction of WIMP dark matter is observed as a nuclear recoil in a specific detector's target material, which in our case is LXe. The main backgrounds (BG) for such nuclear recoil events are electron events (from photoabsorption or Compton scattering of environmental gamma rays), nuclear recoils from the scattering of fast neutrons, and possibly alpha and beta decays in the detector medium itself. The aim of this study is to use the shape of scintillation light pulse in LXe to discriminate against electron events.

The scintillation mechanism is classified into two processes determined by whether or not the process includes recombination [11].

the process without recombination

* Corresponding Author

Email address: ueshima@suketto.icrr.u-tokyo.ac.jp (K.Ueshima).



the process with recombination



Both processes lead to the formation of exciton (Xe_2^*). The de-excitation has two components called singlet and triplet component. The singlet component is caused by a spin singlet state($^1\Sigma_u^+$), and the triplet component is caused by a spin triplet state($^3\Sigma_u^+$) [12].

The shape of the scintillation light pulse in LXe is determined by the lifetimes of the excited states, the time scale of electron-ion recombination, the timing resolution of the photo detector, the time of flight in the detector, and electronics employed to record the scintillation light. The convolution of all these components shapes the recorded scintillation light pulses.

Pulse shape measurements for 1 MeV electrons, α particles and relativistic ions in LXe were reported [13]. In the case of α particles, two distinct lifetime components were observed. The lifetimes for singlet and triplet states were found to be approximately 4 ns and 22 ns respectively. In the case of electron events on the other hand, only one component with 45 ns lifetime was observed.

This pulse shape difference is attributed to the influence of electron-ion recombination [14] [15]. In the case of electron event, dE/dx is one order of magnitude smaller than that in the case of a nuclear recoil [14] [16], and the ensuing ionization is thus spread out over a larger volume. Therefore the recombination process of electron events takes longer than that of nuclear recoil events and dominates the pulse evolution. This hypothesis was confirmed by measurements in electric fields, as the slow component was not observed when an external electric field is applied. Under the influence of an external electric field recombination is suppressed by the drifting apart of the opposing charges, and the two components characteristic of high dE/dx events re-emerge, so that the pulse shape of electron events in an electric field of 4 kV/cm is very close to that of nuclear recoils in zero electric field [12]. In this paper we aim to exploit the characteristically long time constant observed for electron events in LXe at zero electric field.

To this end we examine pulse shape discrimination (PSD) in LXe at energies of less than 20 keV_{ee} (electron equivalent keV). This energy range is most relevant for dark matter searches. The average waveform of nuclear recoil and electron events was previously compared above 10 keV_{ee} [17]. But no event-by-event analysis was done. An event-by-event analysis was reported [18], but the light yield was one order of magnitude lower than our setup. Using dual phase detectors the PSD study was also performed [19]. A reduction factor for electron events of 0.2 by PSD alone was demonstrated at 5 keV_{ee} in a dual phase detector by limiting the electric field to 0.06 kV/cm .

Previous investigations ([17] - [19]) were done at scintillation light yields below 5 p.e./keV (p.e. photoelectrons). Using two closely spaced photomultipliers (PMTs) of the kind also used in the XMASS experiment we measure a light yield of 20.9 p.e./keV , which is expected to us to clearly observe a difference in the pulse shapes of nuclear and electron events even at energies as low as 5 keV_{ee} . Anticipating more limited light collection in real detectors we artificially reduced the photosensitive area in our experimental setup and repeated the measurements at an effective light yield of 4.6 p.e./keV .

2 Detector setup

Our measurements were made in a dedicated setup shown in Fig.1. Two 2 inch hexagonal PMTs (Hamamatsu R10789) facing each other from a distance of 6 cm are viewing the intervening LXe volume from the top and bottom respectively. To the sides the volume is limited by a highly reflective PTFE surface enclosing 0.58 kg of LXe in total. Embedded in the PTFE reflector were a LED and a $300 \text{ Bq } ^{57}\text{Co}$ source. The LED was used to obtain single p.e. spectra and the source to monitor the PMT gain. The light yield from this source was found to be stable within 2% and is incorporated in our systematic uncertainty. To protect the LXe from radioactive contamination this ^{57}Co source was enclosed in a thin stainless steel container.

PMTs, LXe, and the calibration light sources described above were all kept at -100°C inside a stainless steel vessel that itself is suspended inside a vacuum chamber for thermal insulation. Radioactive sources placed outside of the LXe volume and its vacuum enclosure produce the recoil events used in this study: Either a ^{137}Cs source provides gamma rays that produce electron events or a gamma tagged ^{252}Cf fission source provides neutrons to study nuclear recoils. To tag the fission events a plastic scintillator and a PMT (PMT3) were set up next to the Cf source. In the direction of the LXe on the other hand the gamma rays emitted in the ^{252}Cf fission events were shielded by 5 cm of lead.

When filling the setup with LXe the Xe gas was passed through a SAES

getter (Model PS4-MT3-R-1) to remove impurities in the Xe gas. Beyond this no further efforts were made to clean up the high purity Xe used in this experiment.

For data acquisition we used NIM logic to trigger recording of the waveform in a LeCroy WavePro 900 digital oscilloscope as shown in Fig.2. Events in the LXe volume are identified by a coincidence of signals in the two PMTs that view the LXe volume. The width of the coincidence timing window is 100 ns, and the discriminator thresholds were set to 2 p.e. equivalent. As mentioned above a plastic scintillator is used to tag ^{252}Cf fission events every time the Cf source is employed to produce neutron events in the LXe. The corresponding signal from the PMT that reads out the plastic scintillator starts a 140 ns gate that is only for neutron recoil data is also entered into the coincidence unit.

The digital oscilloscope provides 8 bit resolution and a 1 GHz sampling rate. We used it to record 10 μs traces of all PMT signals involved in the respective measurement with 1 ns timing resolution.

The gain of the two PMTs reading out the LXe volume were both set to 3.8×10^6 at the operating temperature of -100°C , with the HV for PMT1 and PMT2 fixed at 1.26 kV and 1.21 kV, respectively. Using the 1 p.e. calibration obtained from the LED data, the fit shown in Fig.3 to the ^{57}Co spectrum determines the energy resolution to be 5.4% (RMS) at 122 keV and the scintillation light yield to be 20.9 p.e./keV_{ee}.

Light collection in real dark matter detectors will be more limited than in this small scale dedicated setup. To quantify the impact of the ensuing loss in statistical power on our discrimination method we artificially reduced the light collection in our setup by covering part of the photocathode area of the bottom PMT (PMT2) with a copper mask. While the PMT1 signal was no longer used to estimate the deposited energy in our study of reduced effective light yield, its signal was used in the trigger during that study in just same way as usual.

The resulting ^{57}Co spectrum is shown in Fig.4, using the p.e. count of only this bottom PMT. The effective light yield was thus reduced to 4.6 p.e./keV_{ee} and the energy resolution to 11.7% (RMS) at 122 keV.

3 Data reduction

A trigger offset of 260 ns allowed us to monitor the baselines 260 ns prior to the recording of our physics events. To clean up both our electron and nuclear recoil event samples we require that none of the events show any “pre-activity”

in the first 150 ns from the beginning of its PMT traces, i.e. from 260 ns to 110 ns prior to the event trigger time.

The dynamic range of oscilloscope was chosen to saturate at a signal height of -400 mV for the PMTs that read out our LXe volume. To avoid problems with saturation, we disregard events where PMT traces from either PMT1 or PMT2 surpass 350 mV, which is roughly equivalent to 1000 p.e. for electron events.

Neutron events are identified by the neutron’s time of flight (TOF) in the offline analysis. Fig.5 shows the TOF distribution extracted from software threshold crossings between the leading edges of PMT3 and PMT2. The software thresholds for all timing determinations corresponds to the typical height of a 3 p.e. signal from the PMTs. The peak at zero timing is due to ^{252}Cf fission gammas passing through the lead shielding set up to suppress such direct gamma interference. To limit the gamma ray background in the sample and specifically select fast neutrons a narrow TOF range from 15 ns to 30 ns was chosen for further analysis.

Table 1 summarizes our data reduction:

	^{252}Cf (neutron) Run	^{137}Cs (gamma ray) Run
before cuts	8.0×10^5	4.0×10^5
after pre-activity cut	5.6×10^5 (69%)	3.5×10^5 (88%)
after saturation cut	2.2×10^5 (27%)	7.4×10^4 (18%)
after TOF selection	2.2×10^4 (2.7%)	

Table 1

Data reduction summary of PSD measurement.

4 Pulse shape discrimination

The parameter we chose to discriminate between electron and nuclear recoil events is the ratio R_{PSD} of scintillation light detected in just the first $\Delta t_{t1} = 20$ ns of the scintillation light pulse, which we refer to as the prompt light, to the total amount of scintillation light detected in that same pulse. As we measure light with PMTs, the amounts of prompt and total light are recorded in units of p.e.: $p.e._{prmt}$ and $p.e._{tot}$. The window for evaluating the amount of total light starts at the same time t_0 as that for the prompt light and is $\Delta t_{tot} = 200$ ns long. t_0 is the same software threshold crossing time as used in the TOF distribution above. Therefore each PMT has its own software threshold crossing resulting in potentially slightly different start times $t_{0,1}$ and $t_{0,2}$ for the integration of a PMT’s respective scintillation signal. The

respective integrals for prompt and total charges measured from the base line subtracted oscilloscope traces $V_{PMT1}(t)$ and $V_{PMT2}(t)$ of the scintillation signal recorded by PMT1 and PMT2 respectively are added as the ratio is evaluated for each event:

$$R_{PSD} = \frac{\int_{t_{0,1}}^{t_{0,1}+\Delta t_{t1}} V_{PMT1} dt + \int_{t_{0,2}}^{t_{0,2}+\Delta t_{t1}} V_{PMT2} dt}{\int_{t_{0,1}}^{t_{0,1}+\Delta t_{tot}} V_{PMT1} dt + \int_{t_{0,2}}^{t_{0,2}+\Delta t_{tot}} V_{PMT2} dt} = \frac{p.e.\text{prmt}}{p.e.\text{tot}} \quad (3)$$

The 20 ns width for the prompt timing window was optimized for best discrimination against gamma recoils. In the case of the reduced effective light yield measurement all terms involving V_{PMT2} are simply dropped. A possible systematic effect of the recoil events position in the LXe volume was studied with the help of the light balance in the two PMTs.

4.1 Neutron data

The recoil energy E_r of a xenon nucleus elastically scattered on by a neutron with energy E_n is expressed by the following equation:

$$E_r = E_n \frac{2(A + 1 - \cos^2 \theta - \cos \theta \sqrt{A^2 - 1 + \cos^2 \theta})}{(1 + A)^2} \quad (4)$$

where A is the mass number of the recoil nucleus, and θ is the scattering angle of the neutron. The maximum recoil energy at $\theta \sim 180^\circ$ is 220 keV_r for an 8 MeV neutron. To estimate the light yield we need to know the relative scintillation efficiency L_{eff} that describes the scintillation light yield of a nuclear recoil event as compared to the yield of an electron event at the same energy; we assume $L_{eff} = 0.2$ [9]. With that the maximum visible energy for a Xe nucleus recoiling in LXe from the elastic scattering of an 8 MeV neutron is 44 keV_{ee}, corresponding to about 920 p.e. in our setup.

The trigger rate for the neutron data run with the ²⁵²Cf source was 13.2 Hz (coincidence rate of PMT1&PMT2&PMT3). The trigger rate of PMT3 alone was 16.2 kHz and the coincidence of just PMT1 and PMT2 occurred at 1.12 kHz.

Accidental coincidences in the sample can be estimated from the background in the TOF distributions for each energy range individually, and are found to be less than 5% after our event selection.

Fig.6 shows the correlation between total p.e. and R_{PSD} for the neutron data. The nuclear recoil band just below $R_{PSD} = 0.5$ can clearly be seen, ending about where expected from the above calculation of maximal recoil energy.

At higher p.e. we also find gamma rays caused by inelastic scattering below $R_{PSD} = 0.4$, which is well separated from the nuclear recoils. The cluster at high $R_{PSD} \sim 0.8$ was caused by very sharp pulse such as Cherenkov light generated in the PMT window.

4.2 Gamma-ray data

Gamma ray data was taken with an external ^{137}Cs source and a lead collimator for the source. The trigger rate of the ^{137}Cs Run was 4.52 kHz (PMT1&PMT2). Fig.7 shows the correlation between total p.e. and R_{PSD} for this electron event sample. While the average R_{PSD} was rather constant for nuclear recoils in the ^{252}Cf data down to low energies, it does increase for gamma-rays at low energies, slowly merging into the nuclear recoil region as recoil energies approach zero.

5 Results

In Fig. 6 and Fig. 7 we expect that power of R_{PSD} to isolate nuclear recoils and reject gamma-ray background is a function of the scintillation light output observed in our recoil event. To estimate the rejection power for gamma-ray background as a function of energy from our data we proceed in three steps: First we split our data sample into energy bands according to the total p.e. count observed with both, PMT1 and PMT2. We then fit Gaussian distributions to both of the R_{PSD} distributions, the one for nuclear recoils and the one for electron events, separately in each energy band. In the third step we estimate the contamination in the nuclear recoil sample from the tail of the gamma-ray Gaussian that extends beyond the mean of the nuclear recoil Gaussian. Using the fitted Gaussians was compared to counting events directly and was found to yield the same result. By integrating the tail of the Gaussian fitted to the electron event distribution that extends beyond the mean of the nuclear recoil R_{PSD} distribution we define the fractional electron leakage r_{EL} into our nuclear recoil sample at an efficiency of 50% for nuclear recoils:

$$r_{EL} = \int_{\mu_n}^{+\text{inf}} G_e dx \quad (5)$$

Here G_e denotes the normalized Gaussian as fitted to the R_{PSD} distribution for electron events, which has a mean μ_e and a variance σ_e . G_n , μ_n , and σ_n stand for the corresponding entities derived from the fit to the R_{PSD} distribution of the nuclear recoils.

Electron leakage was evaluated for the p.e. ranges of 100–150, 150–200, 200–250, 250–300, and 300–400 p.e. Using a conversion factor of 20.9 p.e./keV_{ee}, these p.e. ranges correspond to energy ranges of 4.8–7.2, 7.2–9.6, 9.6–12, 12–14.4, and 14.4–19.1 keV_{ee} respectively. Fig.8 shows the R_{PSD} distributions for both the nuclear and the electron event samples in the energy range from 4.8 to 7.2 keV_{ee}. The corresponding Gaussian fits are also shown.

Fig.9 summarizes the fractional electron leakages we measured in the energy ranges listed above. Horizontal bars reflect the range of electron equivalent recoil energy that was used. Vertical error bars show the statistical uncertainties; the range between the braces has the systematic uncertainties added quadratically. The largest contribution to the systematic uncertainty came from 1 p.e. determination. Open circles show the results for the study with the artificially reduced effective light yield of 4.6 p.e./keV_{ee}, while solid circles show rejection power as a function of energy for the full measured scintillation light yield of 20.9 p.e./keV_{ee}.

The efficiency dependence of the nuclear recoils retention was also studied as shown in Fig.10. The black and red points show the rejection power in the energy range 4.8-7.2 keV_{ee} and 9.6-12 keV_{ee} for non-masked data, respectively. The trade off between rejection of electron events and efficiency for nuclear recoils retention can be evaluated from this figure.

6 Discussion

Our study clearly shows that PSD can be used in purely scintillation based LXe dark matter detectors. As expected its power depends on the effective light yield. Our r_{EL} measure as defined above ultimately depends on the relative size of two quantities: the distance of the two means $\mu_n - \mu_e$ as compared to the width of the electron distribution σ_e .

In Fig.11 we compare the mean values of the R_{PSD} distributions for the electron and nuclear recoil runs as a function of our energy ranges. Both the high yield data and the data taken with an artificially lower effective yield are shown, and it can be seen that the means change by less than 5% as we change the light yield. Yet the effect of this systematic change in $\mu_n - \mu_e$ contributes only 4% to the overall efficiency loss; the larger contribution comes from the widening on the distribution.

Looking at the electron distribution width σ_e , we tried to separate the statistical component reflecting the p.e. statistics from an intrinsic component reflecting the physics of the various processes involved in generating, detecting, conditioning, and recording the signal. Fig.12 and Fig.13 respectively show

σ_e and σ_n , again as a function of our energy ranges.

To estimate the statistical contribution to the width of the R_{PSD} Gaussians we used a Monte Carlo (MC) simulation. In this process we first randomly chose a value for $p.e.tot$ in the relevant range from 50 to 400 p.e.. Using the fits to our R_{PSD} means as shown in Fig.14 we determine the proper R_{PSD} mean to use for this $p.e.tot$ value. Using $p.e.tot$ and its proper R_{PSD} , the MC obtains a set of $p.e.prm$ by sampling from the binomial distribution:

$$P(p.e.prm) =_{p.e.tot} C_{p.e.prm} R_{PSD}^{p.e.prm} (1 - R_{PSD})^{p.e.tot - p.e.prm} \quad (6)$$

From this set of $p.e.prm,MC$ we calculate a set of $R_{PSD,MC} = p.e.prm,MC / p.e.tot$. C means binominal coefficient.

$R_{PSD,MC}$ distributions are built up for both the electron and nuclear recoil means and fitted to Gaussians to extract $\mu_{e,MC}$, $\sigma_{e,MC}$, $\mu_{n,MC}$ and $\sigma_{n,MC}$. The resulting $\mu_{e,MC}$ and $\mu_{n,MC}$ are in good agreement with their measured counterparts μ_e and μ_n .

Fig.12 and Fig.13 show the variances of σ for MC and data compared for electron and nuclear recoil respectively. Systematically the MC data have less spread than the real data, but the effect is quite striking for the high light yield electron event data.

In the case of electron event the waveform is dominated by recombination, which is slow. In case of nuclear recoil, the waveform reflects the relatively short lifetimes of the singlet and triplet states. Fluctuations in the energy deposit along the electron track will translate into fluctuations in the recombination time scale and might be one mechanism by which additional fluctuations can propagate into our R_{PSD} parameter. In an effort to quantify the extra contribution $\sigma_{intrinsic}$ to the width of our distribution that is evident in our data we calculated:

$$\sigma_{intrinsic} = \sqrt{\sigma_e^2 - \sigma_{e,MC}^2} \quad (7)$$

The results are summarized in Fig. 15. The observed consistency in all over energy range gives support to the hypothesis that we are seeing the effects of processes at the light emission stage, as that part was not changed; our light yield was only effectively reduced by a mask. Intrinsically the light yield in the low and high yield data runs was still the same.

7 Conclusion

PSD in liquid xenon was studied at energies relevant to dark matter searches. A significant difference in pulse shape between nuclear recoil and electron events was exploited in a high light yield setup in which 5 keV_{ee} energy deposit produce 100 p.e. in PMT signal output.

At high light yield (20.9 p.e./keV) our R_{PSD} parameter allows a rejection of electron events to a level of $7.7 \pm 1.1(\text{stat}) \pm_{0.6}^{1.2}(\text{sys}) \times 10^{-2}$ in the energy range between 4.8-7.2 keV_{ee} with a 50% efficiency to retain nuclear recoil events. In the energy range 14.4-19.1 keV_{ee} electron events were reduced by more than 3 orders of magnitude with the same efficiency for nuclear recoils.

The dependence of this rejection power on photon statistics was also studied. At low effective light yield (4.6 p.e./keV), a rejection of electron events to $2.4 \pm 0.2(\text{stat}) \pm_{0.2}^{0.3}(\text{sys}) \times 10^{-1}$ was demonstrated for the energy range 4.8-7.2 keV_{ee} with a 50% efficiency for nuclear recoil events.

In our MC replication of the experimental results the width of the R_{PSD} distribution for nuclear recoils is almost exhausted by the expected purely statistical contribution to that width, while that is clearly not the case for electron events. This excess width was tentatively interpreted as stemming from fluctuations inherent to the energy deposit of electron events.

8 Acknowledgements

We gratefully acknowledge the cooperation of Kamioka Mining and Smelting Company. This work was supported by the Japanese Ministry of Education, Culture, Sports, Science and Technology, and Grant-in-Aid for Scientific Research. We are supported by Japan Society for the Promotion of Science.

References

- [1] K. G. Begeman, A. H. Broeils and R. H. Sanders, MNRAS **249**(1991)523.
- [2] J. Dunkley, *et al.*, Astrophys.J.Supp **180**(2009) 306.
- [3] R. A. Knop, *et al.*, Astrophys.J. **598**(2003) 102.
- [4] A. W. Allen, *et al.*, MNRAS **334**(2002) L11.
- [5] M. Tegmark, *et al.*, Phys Rev D **69**(2004) 103501.

- [6] G. Jungman, *et al.*, Phys.Rep. **267**(1996) 195.
- [7] R. Bernabei, *et al.*, Eur.Phys.J.C. **56**(2008) 56.
- [8] Z. Ahmed, *et al.*, Science. **327**(2010) 1619.
- [9] E. Aprile, *et al.*, Phys.Rev.Lett. **105**(2010) 131302.
- [10] Y. Suzuki, arXiv:0008296.
- [11] S. Kubota, *et al.*, J.Phys. **11**(1978)2645.
- [12] S. Kubota, *et al.*, Phys.Rev.B **20**(1979)3486.
- [13] A. Hitachi and T. Takahashi, Phys.Rev.B **27**(1983)5279.
- [14] A. Hitachi, Astropart. Phys. **24**(2005) 247.
- [15] E. Aprile and T. Doke, Rev.Mod.Phys.**82**(2010)2053.
- [16] E. Aprile, *et al.*, Phys.Rev.Lett. **97**(2006) 081302.
- [17] R. Bernabei, *et al.*, Phys.Lett.B **436**(1998)379.
- [18] G. J. Alner, *et al.* Astropart. Phys. **23**(2005)444.
- [19] J. Kwong, *et al.*, Nucl. Instr. and Meth. A **612**(2010)328.

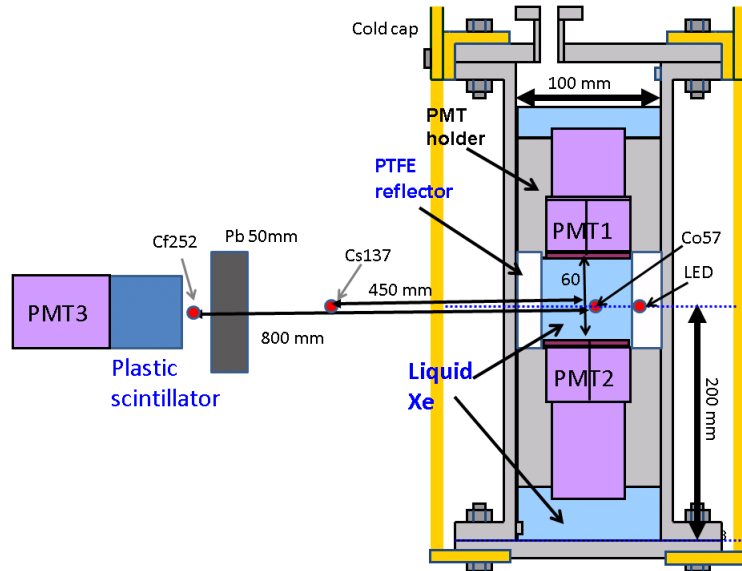


Fig. 1. A schematic view of the detector used in the PSD measurement.

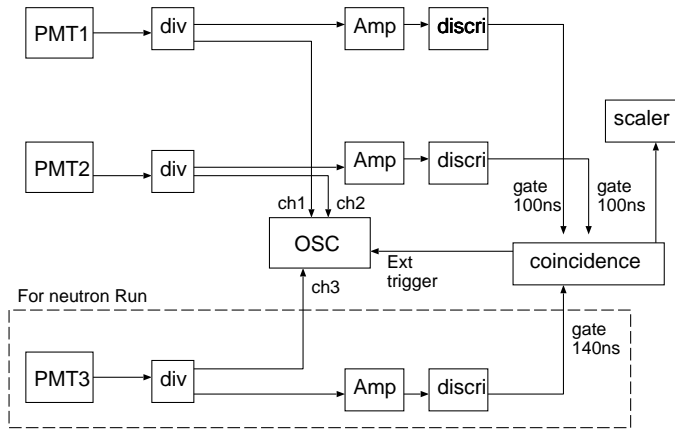


Fig. 2. A schematic diagram of the data acquisition system.

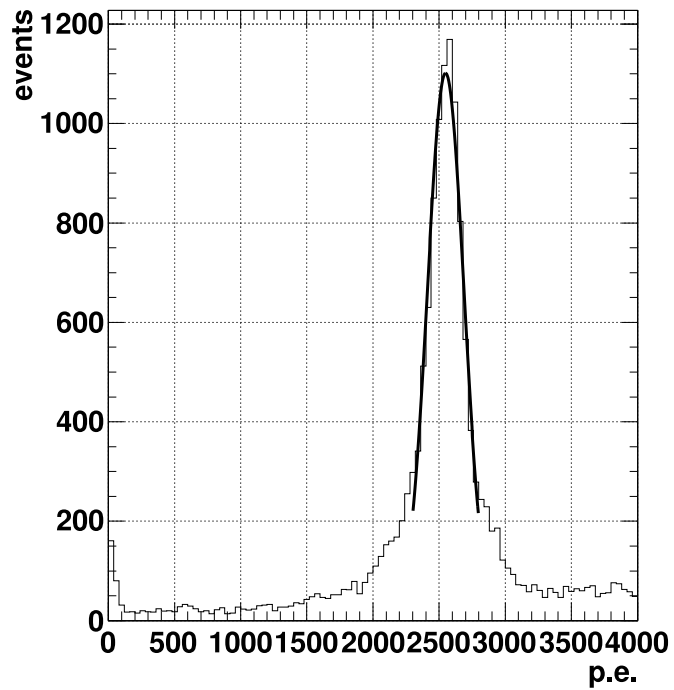


Fig. 3. A typical total p.e. distribution of ^{57}Co data.

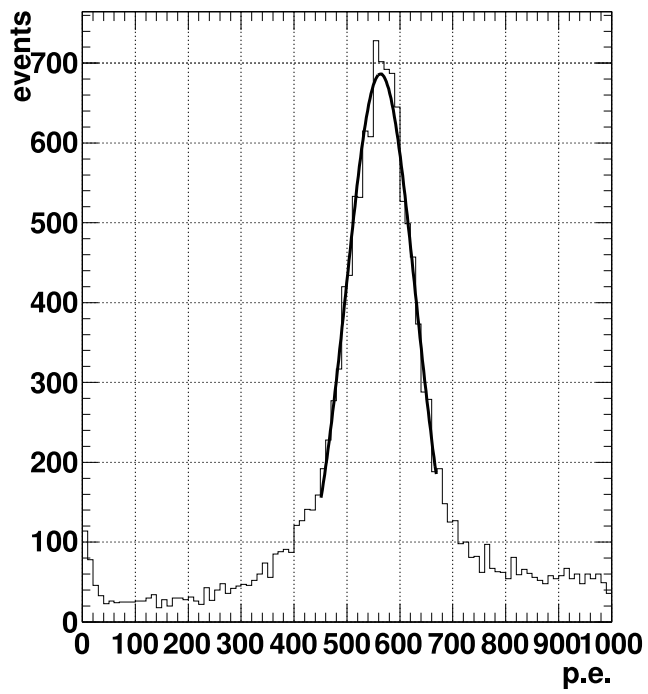


Fig. 4. A typical p.e. distribution of ^{57}Co data for PMT2. The light yield was reduced to 4.6 p.e./keV $_{ee}$ by a mask.

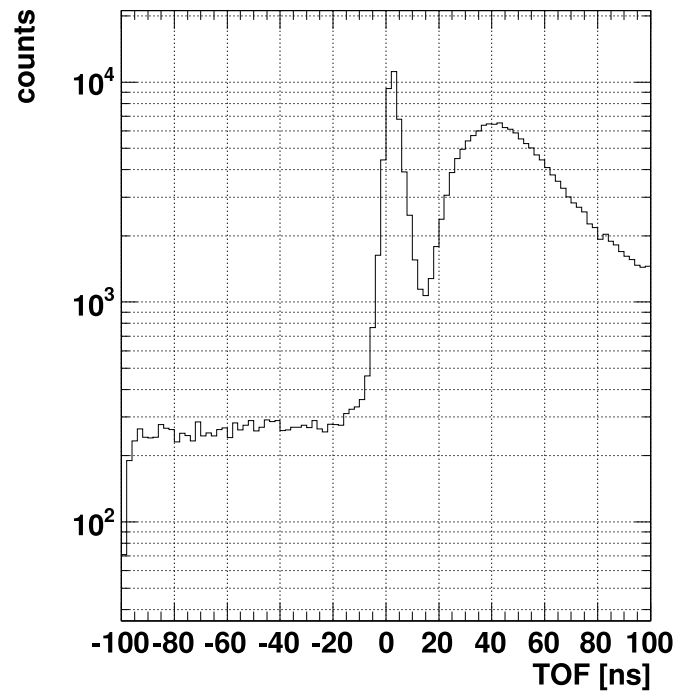


Fig. 5. TOF distribution of ^{252}Cf Run.

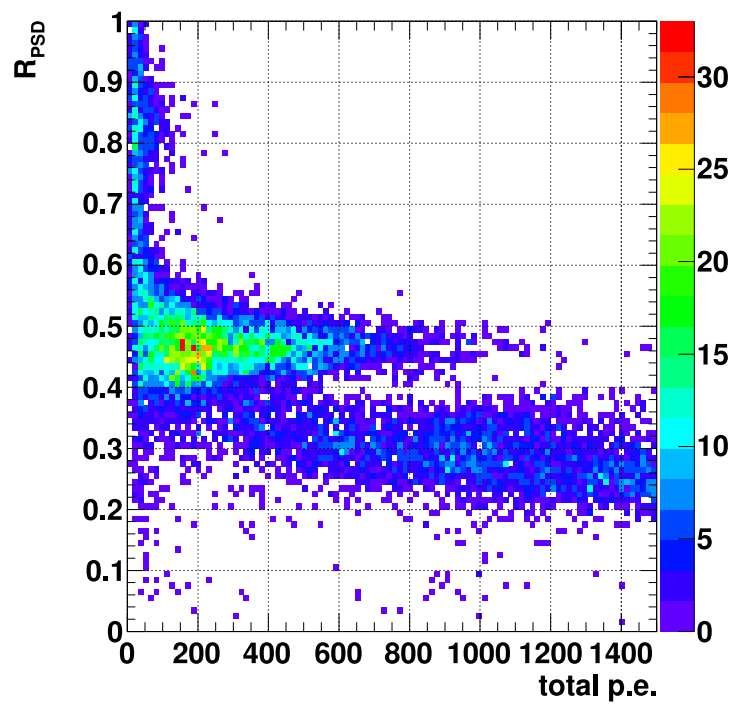


Fig. 6. The scatter plot between total p.e. and R_{PSD} for TOF from 15 to 30 nsec in the ^{252}Cf data.

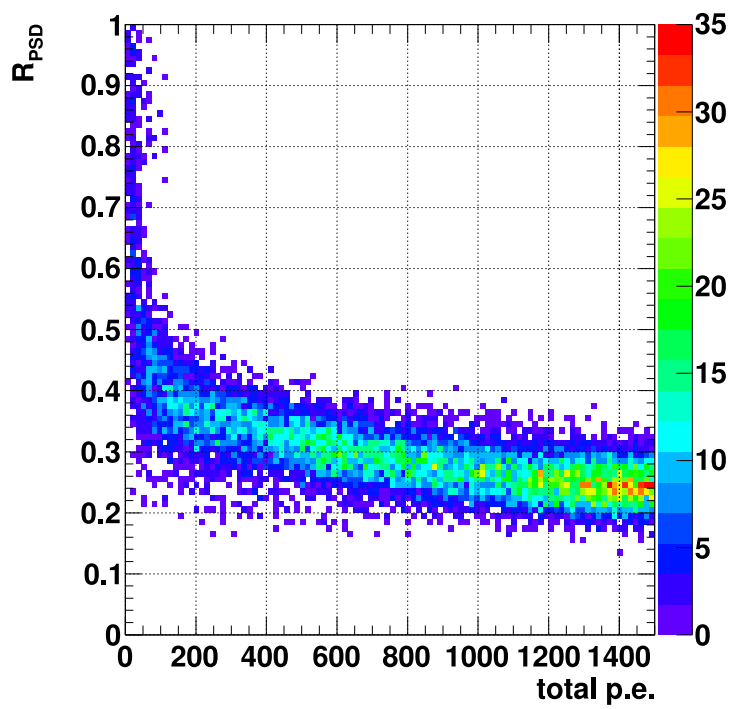


Fig. 7. The ^{137}Cs scatter plot between total p.e. and R_{PSD} .

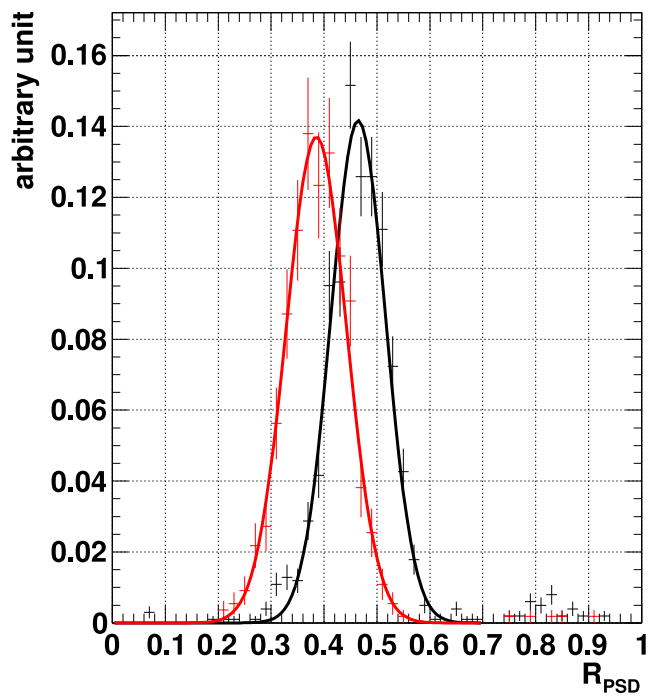


Fig. 8. The R_{PSD} distribution in the energy range between 4.8-7.2 keV $_{ee}$. The red and black lines show the ^{137}Cs data and the ^{252}Cf data, respectively.

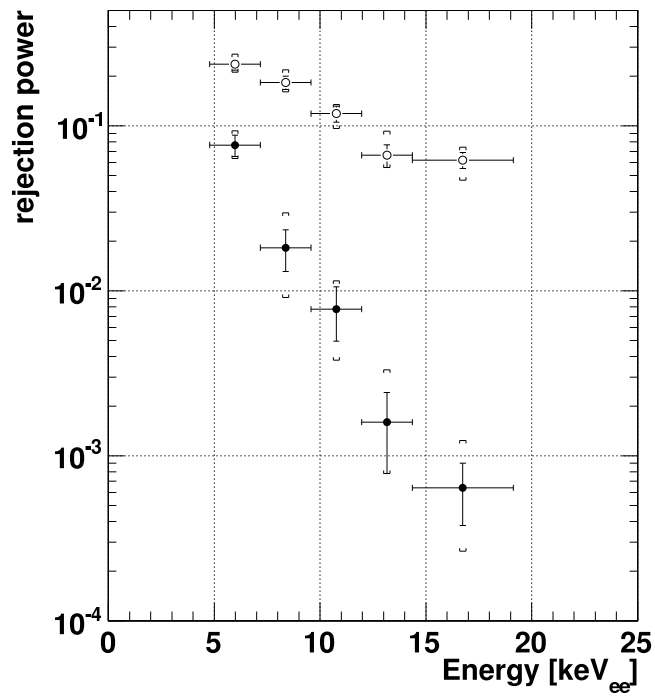


Fig. 9. The rejection power distribution. The open and filled circle points show the masked(4.6 p.e./keV) and non-masked (20.9 p.e./keV) data. Error bars shows the statistical error. Braces show the error including systematic uncertainty added in quadrature.

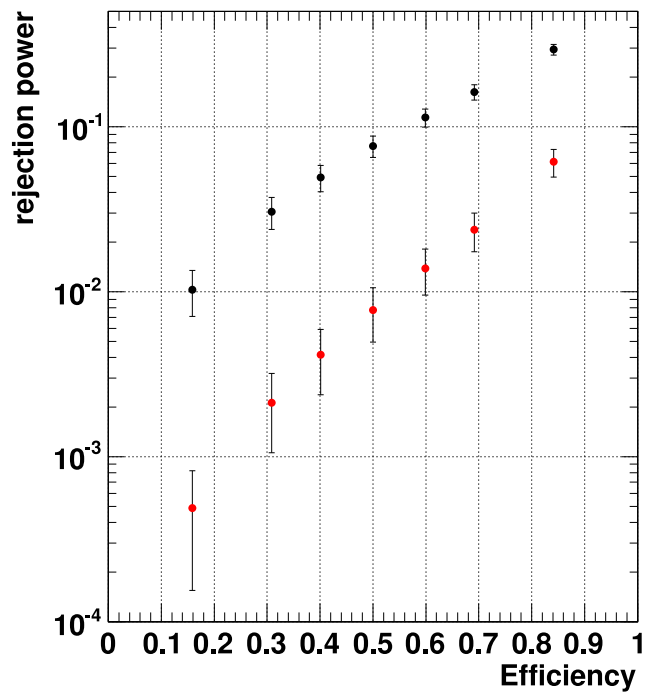


Fig. 10. The efficiency dependence of nuclear recoils retention for rejection power. The black and red points show the rejection power in the energy range 4.8-7.2 keV_{ee} and 9.6-12 keV_{ee} for non-masked data, respectively.

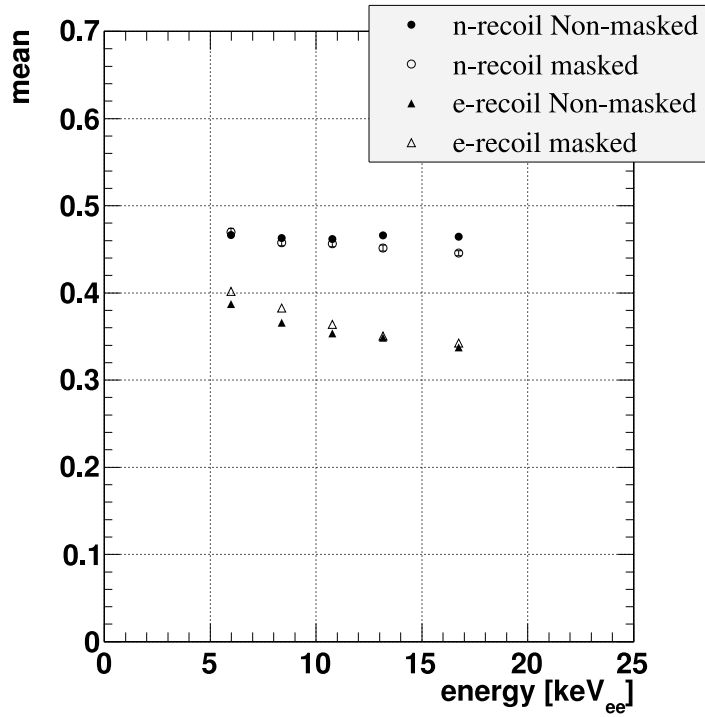


Fig. 11. Mean value of the R_{PSD} as a function of observed energy in unit of keV_{ee} for ^{137}Cs runs and ^{252}Cf runs. The filled and open triangle points show the values of ^{137}Cs runs for the non-masked PMT1+PMT2 (20.9 p.e./keV) and for the masked PMT2 (4.6 p.e./keV), respectively. The filled and open circle points show the values of ^{252}Cf data for the non-masked PMT1+PMT2 (20.9 p.e./keV) and for the masked PMT2 (4.6 p.e./keV), respectively.

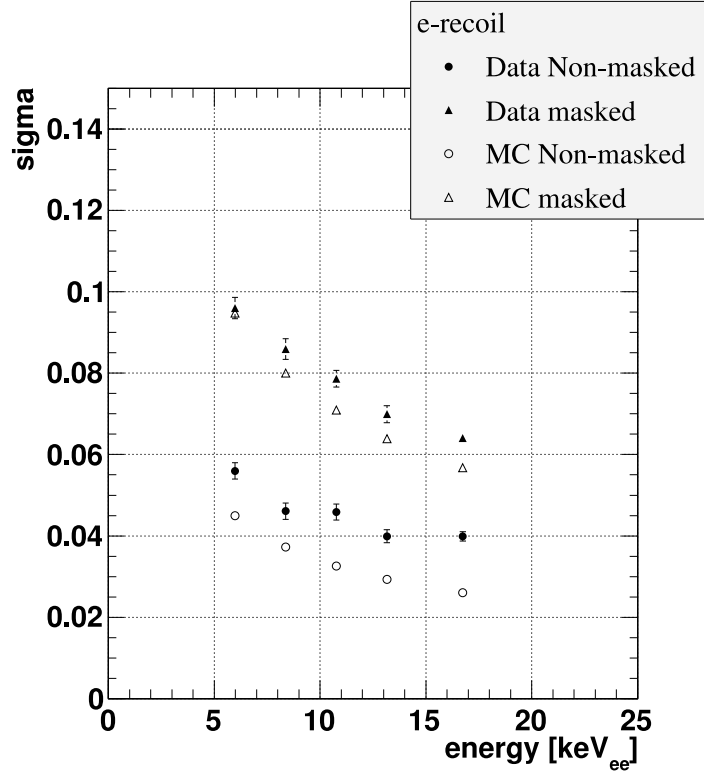


Fig. 12. Sigma of the R_{PSD} distribution as a function of observed energy in unit of keV_{ee} for ^{137}Cs data. The filled circle and filled triangle points show the values for the non-masked PMT1+PMT2 data (20.9 p.e./keV) and for the masked PMT2 data (4.6 p.e./keV), respectively. The open circle and open triangle points show the MC simulation of the non-masked PMT1+PMT2 (20.9 p.e./keV) and the masked PMT2 (light yield was reduced to 4.6 p.e./keV), respectively.

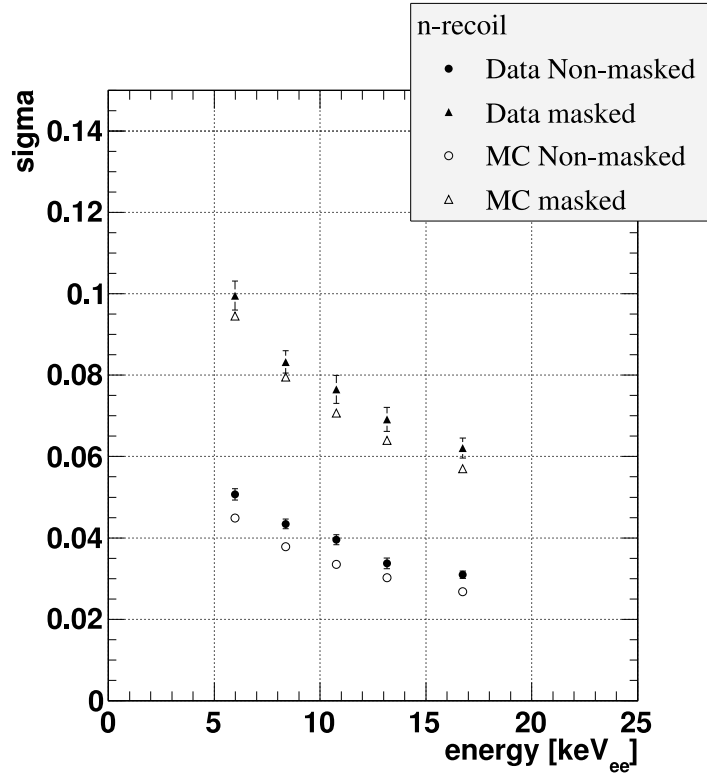


Fig. 13. Sigma of the R_{PSD} distribution as a function of observed energy in unit of keV_{ee} for ^{252}Cf data. The filled circle and filled triangle points show the values for the non-masked PMT1+PMT2 (20.9 p.e./keV) and for the masked PMT2 (4.6 p.e./keV), respectively. The open circle and open triangle points shows the MC simulation of the non-masked PMT1+PMT2 (20.9 p.e./keV) and the masked PMT2 (light yield was 4.6 p.e./keV).

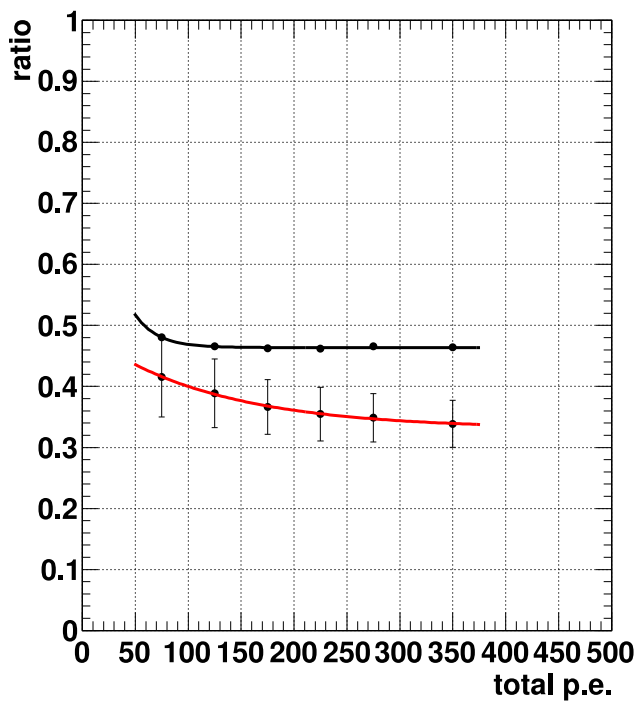


Fig. 14. The relation between R_{PSD} and total p.e. The black and red lines show the fit function of ^{252}Cf and ^{137}Cs . The error bar of ^{137}Cs represent the 1 sigma from the mean value.

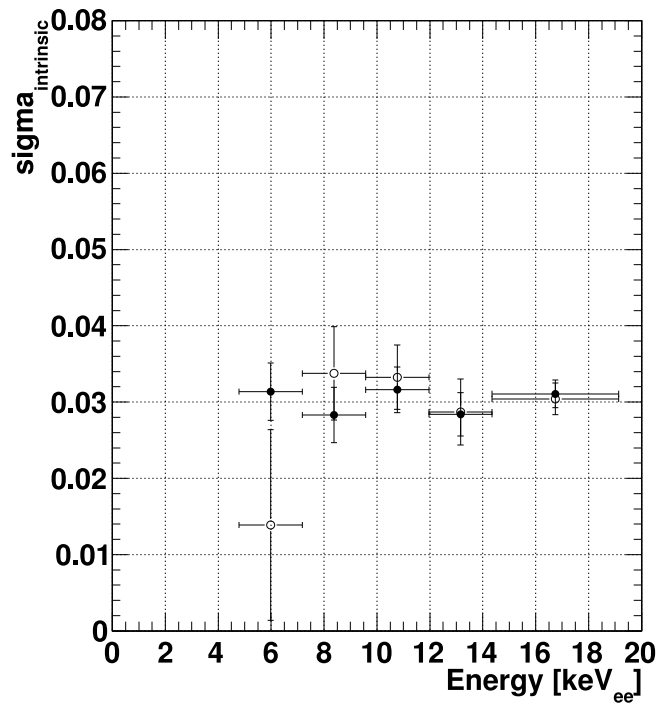


Fig. 15. The $\sigma_{intrinsic}$ distribution of electron events. The open and filled circle points show the values of the masked and the non-masked data, respectively.